THE JOURNAL OF PHYSICAL CHEMISTRY Letters

pubs.acs.org/JPCL Letter

Tailoring the Surface Morphology and Phase Distribution for Efficient Perovskite Electroluminescence

Xuanchi Yu, Tanghao Liu, Qi Wei, Chao Liang, Kaiyang Wang, Jia Guo, Dandan Zhao, Bingzhe Wang, Rui Chen,* and Guichuan Xing*

Cite This: J. Phys. Chem. Lett. 2020, 11, 5877−5882 Read Online

ACCESS | Metrics & More | Article Recommendations | Supporting Information

ABSTRACT: Metal−halide perovskites are promising light-emitting materials due to their continually tunable emission peak, high color purity, high emission efficiency, and low cost. Incorporating some two-dimensional (2D) perovskites into the three-dimensional (3D) perovskite can facilitate carrier localization to the emitting area and reduce nonradiative recombination. However, the incorporated 2D perovskites typically contain diverse phases with different bandgaps and random distribution, which significantly limits the performance of perovskite light emitting diodes (PeLEDs). Furthermore, the morphology of the quasi-2D perovskite film is also a key issue to the device performance. Herein, through replacing part of FA^+ with Cs^+, the phase distribution and morphology of perovskite film can be tailored simultaneously. When 20% of FA^+ is replaced by Cs^+ in the perovskite film, the charge transfer efficiency is enhanced and the current leakage is suppressed. Eventually, the efficiency of PeLED is almost doubled and the stability is also significantly improved.

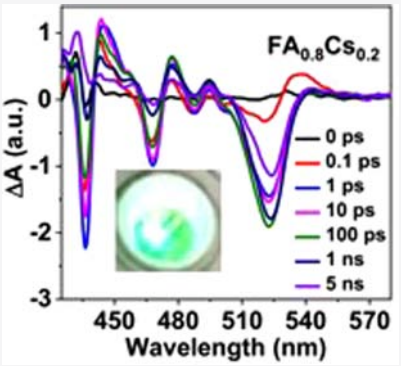

In the past decade, metal−halide perovskites have achieved great success in various areas, including solar cells, light emitting diodes (LEDs), lasers, and so on.[1−4] Compared with traditional LEDs, perovskite light emitting diodes (PeLEDs) show advantages of continually tunable emission peak, high color purity, easy-fabrication, and low cost. Therefore, they have attracted increasing research interests.[5−7] Nowadays, the record external quantum efficiencies (EQEs) of near-infrared, red, and green PeLEDs have all exceeded 20%,[8−10] and the EQE of blue PeLED has also exceeded 10%.[11] Three-dimensional (3D) perovskites generally possess long and balanced charge diffusion lengths, which is their key advantage in solar cells.[12,13] However, this feature is not favorable for light emitting since the long diffusion length increases the probability of nonradiative recombination under current injection. For the sake of rapid radiative recombination, it is expected that charge carriers could be confined in a small region.[14] Quantum dot, nanocrystalline, and quantum well (QW) can all meet this requirement.[15−18] Among these low-dimensional nanostructures, QW possesses the simplest preparation procedure, which could be deposited by incorporating suitable long-chain cations into the perovskite precursor solution.

In two-dimensional (2D) perovskite, the inorganic $[MX_6]^{4-}$ octahedral slabs are sandwiched by two long organic barrier layers. Due to thermodynamic stability of the perovskite compounds in solution, the quasi-2D perovskite films deposited with solution methods typically consist of multiple QWs with random well width (inorganic layer number, n) distribution.[19] 3D perovskite can be viewed as an extreme case of high-n QW ($n = \infty$). Low-n QWs possess a wide bandgap and high exciton binding energy, which is necessary for confining charge carrier diffusion. However, charge carriers captured by these low-n QWs can hardly transfer to $n = \infty$ phase for emission, thus lowering the charge-to-photon conversion efficiency. For these materials, manufacturing stable and efficient LEDs with high brightness and color purity is still a big challenge. Therefore, tailoring the phase distribution is desired to balance the charge confine and diffusion.

Herein, we choose formamidinium lead bromide ($FAPbBr_3$) as the light emitter and employ the (2-phenylethyl)ammonium cation (PEA^+) as the long-chain cation to construct quasi-2D perovskite. The one-step spin-coating method with antisolvent washing is adopted to deposit perovskite films. Through replacing part of FA^+ with Cs^+ at the A-site, we can tune the morphology and phase distribution of quasi-2D perovskite films. When the Cs^+ content is 20%, the perovskite film with compact surface and improved phase distribution is obtained. In this film, the charge transfer from the wide band gap phase to the 3D phase is enhanced and current leakage is suppressed. The PeLED with 20% Cs^+ can deliver an EQE of 4.5%, a luminance of near 10000 cd/m^2, and improved stability. The

Received: April 24, 2020
Accepted: June 25, 2020
Published: June 25, 2020

https://dx.doi.org/10.1021/acs.jpclett.0c01252
J. Phys. Chem. Lett. 2020, 11, 5877−5882

correlation between film structure and electroluminescence (EL) is studied in detail by morphology characterization and ultrafast spectroscopy.

As reported by many literatures, $FAPbX_3$ (X = Cl, Br, I) perovskites are a class of materials with excellent optoelectronic properties and high thermal stability.[17,20−23] However, the desired cubic phase can hardly keep stable and the formation energy is high.[20,24] The reason can be explained by the Goldschmidt tolerance factor (t), which is an empirical index to predict the preferential crystal structure of materials with ABX_3 formula. The expression of Goldschmidt tolerance factor is $t = (r_A + r_X)/\sqrt{2}(r_B + r_X)$, where r_A, r_B, and r_X are radii of the A cation, B cation, and X anion, respectively. Perovskite materials tend to form a cubic structure when $0.8 < t < 1$. The tolerance factor of $FAPbBr_3$ is calculated to be 1.008, slightly larger than 1. Hence, the formation of cubic $FAPbBr_3$ and similar high-n phases are not preferred during the growth of quasi-2D perovskite film. As a result, there would be large quantities of low-n phases in the final film, which is not favorable for efficient electroluminescence. The radius of Cs^+ is smaller than that of FA^+. Replacing part of FA^+ with Cs^+ can lower the effective tolerance factor.[25] Here, we tune the ratio of Cs^+ to FA^+ in the precursor solution to modulate the growth of quasi-2D perovskite films. According to the Cs^+ content (x), the films are denoted as $FA_{1-x}Cs_x$.

Scanning electron microscopy (SEM) measurements are performed to study surface morphologies of these quasi-2D perovskite films. As shown in Figure 1a, there are lots of pinholes on the surface of the FA film, which may lead to serious current leakage in PeLED. By contrast, the $FA_{0.8}Cs_{0.2}$ film and $FA_{0.6}Cs_{0.4}$ film exhibit compact and uniform surfaces (Figures 1b,c). In $FA_{0.6}Cs_{0.4}$ film, there are some thin nanoplates insert vertically. These nanoplates are 2D perovskites.[26] In the $FA_{0.8}Cs_{0.2}$ film, similar nanoplates are rarely found. The differences in morphology indicate that the A-cation can modulate the crystallization dynamics of the quasi-2D perovskite. In general, pinholes in the perovskite film are induced by the slow crystallization rate.[27] The introduction of Cs^+ reduces the formation energy and accelerates the crystallization, resulting in a compact perovskite film. When Cs^+ content is increased to 40%, the compact surface of perovskite film is still retained. Meanwhile, the growth of low-n phases is also promoted. Crystal structures of these perovskite films are studied by X-ray diffraction (XRD) (Figure S1). Compared with the XRD pattern of the FA film, a new and weak diffraction peak (15.08°) appears in the XRD pattern of $FA_{0.8}Cs_{0.2}$ film. According to previous literature, it is ascribed to $CsPbBr_3$.[8] In the XRD pattern of the $FA_{0.6}Cs_{0.4}$ film, the peak becomes much stronger. It means 40% Cs^+ cannot mix evenly with FA^+ and finally results in seriously phase segregation. Since the solubility of $CsPbBr_3$ is much lower than that of $FAPbBr_3$, $CsPbBr_3$ precipitates earlier during spin coating, thus leaving a high ratio of PEA^+ to FA^+ in the solution, which is the reason for many low-n phases in the $FA_{0.6}Cs_{0.4}$ film. To precisely evaluate the uniformity of these films, atomic force microscopy (AFM) images of these films are also tested and shown in Figure 1d−f. In a 2 μm × 2 μm aperture, root-mean-square roughnesses (RMSs) of FA, $FA_{0.8}Cs_{0.2}$, and $FA_{0.6}Cs_{0.4}$ are 16.3, 14.6, and 13.2 nm, respectively. It implies that the higher Cs^+ content, the smoother the perovskite film. The smoother surface of perovskite film is easier to be completely covered by a charge inject layer on the top, which is also helpful for reducing the current leakage of PeLED.

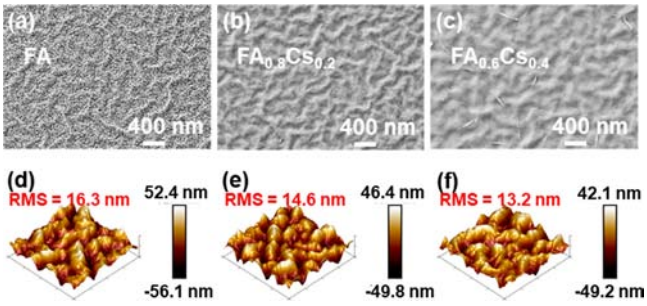

Figure 1. Top-view SEM images of the (a) FA film, (b) $FA_{0.8}Cs_{0.2}$ film, and (c) $FA_{0.6}Cs_{0.4}$ film. 3D AFM images of (d) the FA film, (e) the $FA_{0.8}Cs_{0.2}$ film, and (f) the $FA_{0.6}Cs_{0.4}$ film.

Figure 2a exhibits the UV−visible absorption spectra of FA, $FA_{0.8}Cs_{0.2}$, and $FA_{0.6}Cs_{0.4}$ films. All these spectra show similar absorption edges at 530 nm and strong exciton absorption peaks at 430 nm. The absorption edge at 530 nm is consistent with the bandgap of $FA_{1-x}Cs_xPbBr_3$ (2.3 eV). According to the report of Li et al., Cs^+ content has no influence on the bandgap of mixed cation perovskite.[25] The absorbance of Cs^+ contained films is weaker than that of the FA film in all the absorption range. Absorption coefficients of FA, $FA_{0.8}Cs_{0.2}$, and $FA_{0.6}Cs_{0.4}$ films at 400 nm are 3.6×10^4, 3.4×10^4, and 3.2×10^4 cm^{-1}, respectively. The absorption peak at 430 nm is attributed to the $n = 2$ phase.[28,29] In the absorption spectra of three films, the peaks at 430 nm are very strong, revealing the formation of much $n = 2$ phase in all films. Meanwhile, the peak at 470 nm is the strongest in the absorption spectra of $FA_{0.8}Cs_{0.2}$ film. FA and $FA_{0.6}Cs_{0.4}$ films also show absorption peaks at 470 nm, but

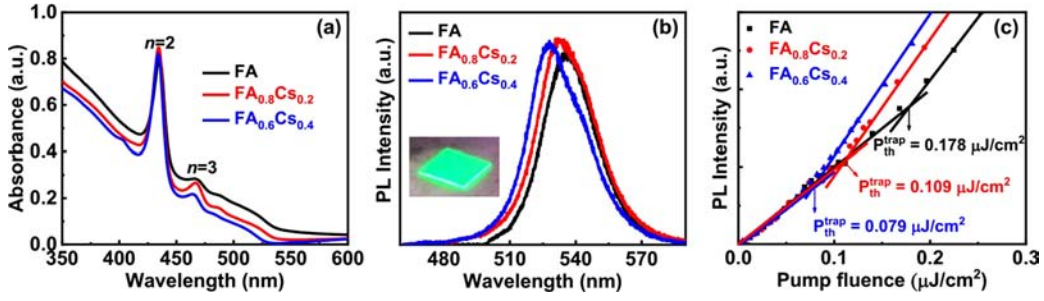

Figure 2. (a) UV−visible absorption spectra, (b) PL spectra, and (c) pump fluence dependent PL intensity of various perovskite films. The PL spectra are pumped by 400 nm excitation.

https://dx.doi.org/10.1021/acs.jpclett.0c01252
J. Phys. Chem. Lett. 2020, 11, 5877−5882

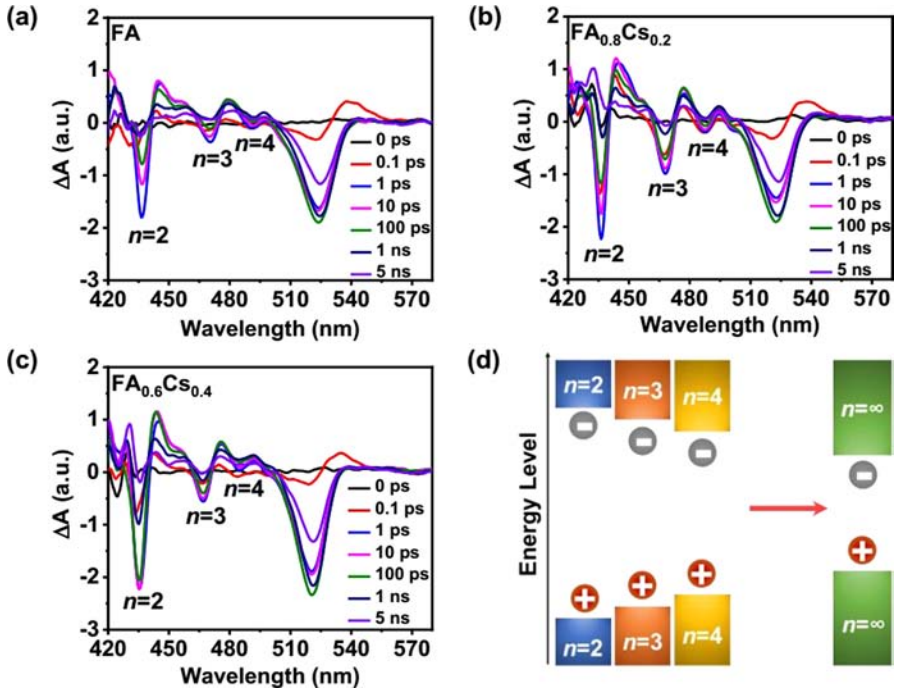

Figure 3. TA spectra of (a) FA, (b) $FA_{0.8}Cs_{0.2}$, and (c) $FA_{0.6}Cs_{0.4}$ films. (d) Schematical diagram of energy levels and charge transfer behaviors in quasi-2D perovskite. The TA spectra are collected under 400 nm excitation.

very weak. It means a proper amount of Cs^+ can promote the formation of the n = 3 phase. Too much or too little Cs^+ will lead to the lack of high-n 2D phases (n = 3, 4). Photoluminescence (PL) spectra of these films are tested under 400 nm excitation (100 fs, 1 kHz, 1 μJ cm^{-2}). As shown in Figure 2b, the PL peak blue shifts with the increase of Cs^+ content. The PL intensities of $FA_{0.8}Cs_{0.2}$ film and $FA_{0.6}Cs_{0.4}$ film are slightly higher than that of FA film. To precisely evaluate their PL property, photoluminescence quantum yield (PLQY) values of the three films are tested under an excitation of 365 nm. FA, $FA_{0.8}$, and $FA_{0.6}$ delivers PLQY values of 15%, 20%, and 19%, respectively. It may be concluded that the incorporation of Cs^+ enhances light emission. To further clarify the background mechanism, the PL spectra were collected with varied pump fluence. The correlation between PL intensity and pump fluence is displayed in Figure 2c. Since part of the photogenerated charge carriers would fill in trap states in perovskite, the increase of PL intensity with the pump fluence is relatively slow under low excitation density. With the increase of pump fluence, all trap states would be filled. Then, the PL intensity increases faster with the increase of pump fluence. The increasing speed of PL intensity is reflected by the slope in Figure 2c. The trap density can be extracted from the point where trap states are first fully filled. The calculated trap densities of FA, $FA_{0.8}Cs_{0.2}$, and $FA_{0.6}Cs_{0.4}$ are 1.29×10^{16}, 0.74×10^{16}, and 0.51×10^{16} cm^{-3}, respectively. Time-resolved photoluminescence (TRPL) is also adopted to evaluate the film quality. The tested results and fitted curves are shown in Figure S2. The effective lifetimes of FA, $FA_{0.8}$, and $FA_{0.6}$ films extracted from TRPL decay curves are 13.1, 11.2, and 9.7 ns, respectively. The short carrier lifetimes of Cs^+ contained perovskite films are beneficial for the rapid radiative recombination.

To reveal the charge carrier dynamics and detailed phase distribution in these perovskite films, transient absorption (TA) measurements were conducted under a 400 nm pulse excitation (1 kHz, 100 fs, 2.4 μJ/cm^2). Panels a–c of Figure 3 show the TA spectra at a series of selected delay times. It is found that there are multiple perovskite phases in these perovskite films. In all three spectra, strong photobleaching (PB) peaks related to the n = 2 phase (430 nm) and 3D phase (~525 nm) can be clearly seen. The PB peaks at 470 and 490 nm correspond to the n = 3 and n = 4 phases, respectively. It is observed that the recovery of n = 2, 3, and 4 PB peaks is accompanied by the increment of the n = ∞ PB peak. It indicates carrier/energy transfer from 2D phases to the n = ∞ phase in the film, as exhibited in Figure 3d. The n = 3 peak of $FA_{0.6}Cs_{0.4}$ film is a bit stronger than that of the n = 3 peak of the FA film. However, they are both very weak. Meanwhile, n = 4 peaks are also weak and overlapped by photoinduced-absorption signals in TA spectra of FA film and $FA_{0.6}Cs_{0.4}$ film. Thus, n = 4 peaks are nearly unobservable in Figure 3a,c. Only in the TA spectra of the $FA_{0.8}Cs_{0.2}$ film is the intensity of the n = 3 peak as high as half of that of the n = 2 peak, and the n = 4 peak is also observed. The increased n = 3, 4 phases lead to a better graded energy level landscape, which is favorable for carrier/energy transfer from the n = 2 phase to the n = ∞ phase.[30] To confirm this, bleaching kinetics of n = 2 peaks in three films are extracted and fitted with the multiexponential function (Figure S3). The lifetimes are summarized in Table S1. The n = 2 PB peak of $FA_{0.8}Cs_{0.2}$ film decays much faster than those of FA and $FA_{0.6}Cs_{0.4}$ films, revealing the effective carrier/energy transfer in $FA_{0.8}Cs_{0.2}$ film. Based on the TA analysis, it is expected that the $FA_{0.8}Cs_{0.2}$ film is the most suitable for high-performance PeLED.

Using FA, $FA_{0.8}Cs_{0.2}$, and $FA_{0.6}Cs_{0.4}$ films as emission layers, we fabricate PeLEDs with the structure of ITO/poly(2,3-dihydrothieno-1,4-dioxin)–poly(styrenesulfonate) (PEDOT:PSS)/perovskite/2,2′,2″-(1,3,5-benzinetriyl)tris(1-phenyl-1*H*-benzimidazole) (TPBi)/LiF/Al. The device structure and working principle are schematically illustrated in Figure 4a,b, respectively. Panels c–f of Figure 4 present performances

https://dx.doi.org/10.1021/acs.jpclett.0c01252
J. Phys. Chem. Lett. 2020, 11, 5877–5882

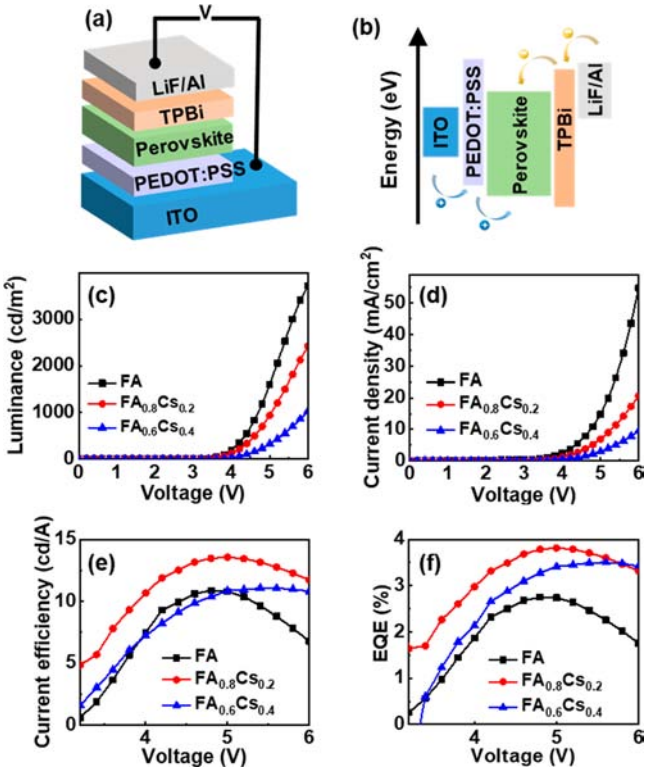

Figure 4. (a) Device structure and (b) working principle of the PeLED in this work. (c) Luminance–voltage (L–V) curves. (d) Current density–voltage (J–V) curves. (e) Current efficiency–voltage (CE–V) curves. (f) EQE–voltage (EQE–V) curves of various PeLEDs.

of various PeLEDs. The luminance decreases with the increase of Cs^+ content in the full bias range. Under the same bias, the current density of the FA based PeLED is much higher than those of $FA_{0.8}Cs_{0.2}$ and $FA_{0.6}Cs_{0.4}$ based PeLEDs, which should be mainly ascribed to pinhole induced current leakage. This is in accordance with the prediction of morphology characterization. Moreover, the charge injection in $FA_{0.6}Cs_{0.4}$ is lower than that in $FA_{0.8}Cs_{0.2}$, which explains the lower luminance. The low charge injection in $FA_{0.6}Cs_{0.4}$ is caused by phase segregation and too much n = 2 phase. As a result, the $FA_{0.8}Cs_{0.2}$ based PeLED delivers the highest CE of 13.8% and an EQE of 3.8%, much higher than those of FA and $FA_{0.6}Cs_{0.4}$ PeLEDs. Detailed parameters of these devices are displayed in Table 1.

Table 1. Parameters of Various PeLEDs

	Von (V)	J@6 V (mA/cm^2)	luminance (cd/m^2)	CE (cd/A)	EQE (%)
FA	3	55	3888	10.8	2.5
$FA_{0.8}Cs_{0.2}$	3	21	3039	13.6	3.8
$FA_{0.6}Cs_{0.4}$	3	10	1804	11.1	3.3
$FA_{0.8}Cs_{0.2}$ (best)	3	95	9050	17.7	4.5

Through further optimizing the charge injection layers and device fabrication procedure, the EQE of the $FA_{0.8}Cs_{0.2}$ based PeLED can be boosted to 4.5% (Figure 5a). Specifically, the evaporation speed of TPBi is optimized to be 0.5 ± 0.1 Å/s. Before depositing perovskite films, the glovebox is purged with nitrogen and the temperature of glovebox is fixed at 28 ± 2 °C.

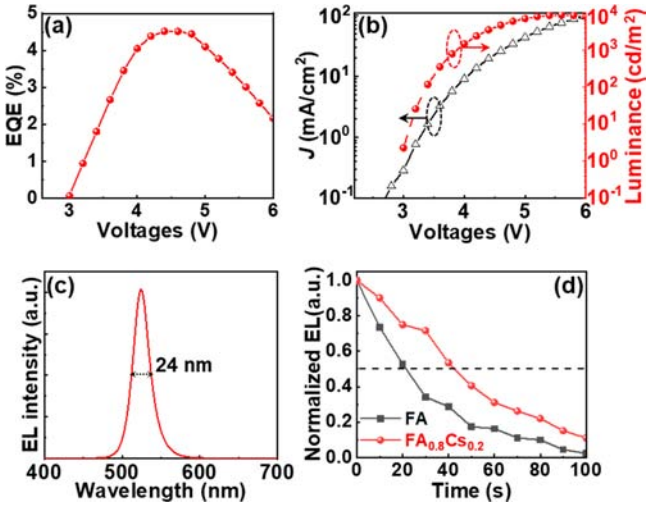

Figure 5. (a) Relationship between EQE and voltage of the best-performance PeLED. (b) J–V–L curve of the best-performance PeLED. (c) EL spectra of the best-performance PeLED under a bias of 5 V. (d) Luminance evolution of FA and $FA_{0.8}Cs_{0.2}$ based PeLEDs under a voltage of 5 V.

The J–V–L curve of the champion device is exhibited in Figure 5b. The highest luminance is approaching 10000 cd/m^2. The EL spectrum of this device under a bias of 5 V is exhibited in Figure 5c. It centers at 528 nm with a full width at half-maximum (fwhm) of 24 nm, showing high color purity. The Commission Internationale de l'Eclairage (CIE) chromaticity coordinate (x, y) is calculated to be (0.1598, 0.7621) (Figure S4). Moreover, the device stability is also studied by monitoring the luminance under a bias of 5 V. The luminance of FA based PeLED degrades to half of the initial value in 20 s, while $FA_{0.8}Cs_{0.2}$ based PeLED keeps more than half of its initial luminance for 42 s (Figure 5d). It means that Cs^+ incorporation improves not only the EQE but also the stability of PeLED.

EXPERIMENTAL SECTION

Materials and Reagents. $PbBr_2$, FABr, CsBr, PEABr, PEDOT:PSS, TPBi, and LiF were purchased from Xi'an Polymer Light Technology Corp. DMSO and CB were purchased from Sigma-Aldrich. All chemicals were used as received without further purification.

Precursors and Films Preparation. $PEA_2(FAPbBr_3)_2PbBr_4$ solution was prepared by dissolving PEABr, FABr, and $PbBr_2$ with a molar ratio of 2:2:3 and Pb^{2+} concentration of 0.5 M in DMSO. For $FA_{0.8}Cs_{0.2}$ and $FA_{0.6}Cs_{0.4}$ solutions, 20% and 40% of FABr in the above recipe was replaced by CsBr, respectively. All precursor solutions were shaken for at least 30 min and filtered with 0.22 μm polytetrafluoroethylene (PTFE) filter before use. Perovskite films were deposited by spin coating precursor solution at 3000 rpm for 120 s and dropping 100 μL of CB onto spinning films at 30 s. Then, the as-deposited films were annealed at 90 °C for 60 min.

Fabrication of PeLEDs. The prepatterned ITO-coated glasses were sequentially cleaned with diluted detergent, deionized water, acetone, and 2-propanol (IPA) and treated in a UV–ozone cleaner for 10 min. PEDOT:PSS was spin coated on top of ITO at 4000 rpm for 60 s followed by annealing at 120 °C for 30 min in the ambient atmosphere. Then, the samples were transferred into the N_2-filled glovebox. Perovskite films were

https://dx.doi.org/10.1021/acs.jpclett.0c01252
J. Phys. Chem. Lett. 2020, 11, 5877–5882

deposited according to the procedure described above. Subsequentially, TPBi (40 nm), LiF (1 nm), and Al (80 nm) were evaporated sequentially with a 2 mm × 2 mm shadow mask.

Characterization. XRD patterns were tested by a Rigaku (RINT-2500) X-ray diffractometer (Cu Ka radiation, λ = 1.5418 Å). SEM images were measured by a field emission scanning electron microscope (JEM-7500F). AFM images were measured by a Dimension Fastscan Atomic Force Microscope (Bruker Fastscan). UV−vis−NIR absorption spectra were recorded by a Shimadzu UV 3600 spectrophotometer. PL (excitation at 400 nm) was measured with Hamamatso spectrometer. *J*−*V*−*L* curves were collected by a Hamamatsu spectrometer in combination with a Keithley 2400 source meter. The TA spectra were measured by employing the HELIOS TA system. The 400 nm laser pulses were generated by passing the strong 800 nm femtosecond laser beam through a BBO crystal.

In summary, we prepared FA-based quasi-2D perovskite and replaced part of FA^+ with Cs^+. The correlations between Cs^+ content and the surface morphology and phase distribution of quasi-2D perovskite film are demonstrated. It is found that the incorporation of Cs^+ improves surface coverage and uniformity of the perovskite film. Too much or little Cs^+ leads to the lack of n = 3, 4 phases, which is not favorable for electroluminescence. A 20% Cs^+ sample can facilitate the formation of a better graded energy level landscape, resulting in efficient charge transfer. By incorporating 20% Cs^+, the PeLED delivers a doubled EQE of 4.5% and enhanced stability. These results provide a simple way to improve the performance of PeLEDs.

■ ASSOCIATED CONTENT

Supporting Information

The Supporting Information is available free of charge at https://pubs.acs.org/doi/10.1021/acs.jpclett.0c01252.

XRD, time-resolved photoluminescence (TRPL) curves, TA kinetic results, lifetimes of n = 2 peaks, and Commission Internationale de l' Eclairage (CIE) coordinates (PDF)

■ AUTHOR INFORMATION

Corresponding Authors

Guichuan Xing − *Joint Key Laboratory of the Ministry of Education, Institute of Applied Physics and Materials Engineering, University of Macau, Avenida da Universidade, Taipa, Macau 999078, China;* orcid.org/0000-0003-2769-8659; Email: gcxing@um.edu.mo

Rui Chen − *Department of Electrical and Electronic Engineering, Southern University of Science and Technology, Shenzhen, Guangdong 518055, China;* orcid.org/0000-0002-0445-7847; Email: chenr@sustech.edu.cn

Authors

Xuanchi Yu − *Joint Key Laboratory of the Ministry of Education, Institute of Applied Physics and Materials Engineering, University of Macau, Avenida da Universidade, Taipa, Macau 999078, China; Department of Electrical and Electronic Engineering, Southern University of Science and Technology, Shenzhen, Guangdong 518055, China*

Tanghao Liu − *Joint Key Laboratory of the Ministry of Education, Institute of Applied Physics and Materials Engineering, University of Macau, Avenida da Universidade, Taipa, Macau 999078, China*

Qi Wei − *Joint Key Laboratory of the Ministry of Education, Institute of Applied Physics and Materials Engineering, University of Macau, Avenida da Universidade, Taipa, Macau 999078, China*

Chao Liang − *Joint Key Laboratory of the Ministry of Education, Institute of Applied Physics and Materials Engineering, University of Macau, Avenida da Universidade, Taipa, Macau 999078, China*

Kaiyang Wang − *Joint Key Laboratory of the Ministry of Education, Institute of Applied Physics and Materials Engineering, University of Macau, Avenida da Universidade, Taipa, Macau 999078, China*

Jia Guo − *Joint Key Laboratory of the Ministry of Education, Institute of Applied Physics and Materials Engineering, University of Macau, Avenida da Universidade, Taipa, Macau 999078, China*

Dandan Zhao − *Joint Key Laboratory of the Ministry of Education, Institute of Applied Physics and Materials Engineering, University of Macau, Avenida da Universidade, Taipa, Macau 999078, China*

Bingzhe Wang − *Joint Key Laboratory of the Ministry of Education, Institute of Applied Physics and Materials Engineering, University of Macau, Avenida da Universidade, Taipa, Macau 999078, China*

Complete contact information is available at: https://pubs.acs.org/10.1021/acs.jpclett.0c01252

Notes

The authors declare no competing financial interest.

■ ACKNOWLEDGMENTS

X.Y., T.L., and Q.W. contributed equally to this work. The authors acknowledge the Science and Technology Development Fund, Macao SAR (File no. FDCT-0044/2020/A1, FDCT-091/2017/A2, FDCT-014/2017/AMJ), UM's research fund (File no. MYRG2018-00148-IAPME), the Natural Science Foundation of China (91733302, 61935017), Natural Science Foundation of Guangdong Province, China (2019A1515012186), and Guangdong-Hong Kong-Macao Joint Laboratory of Optoelectronic and Magnetic Functional Materials (2019B121205002). R.C. acknowledges the funding support from Shenzhen Science and Technology Innovation Commission (Projects Nos.: KQJSCX20170726145748464, JCYJ20180305180553701, and KQTD2015071710313656).

■ REFERENCES

(1) Kojima, A.; Teshima, K.; Shirai, Y.; Miyasaka, T. Organometal Halide Perovskites as Visible-Light Sensitizers for Photovoltaic Cells. *J. Am. Chem. Soc.* **2009**, *131*, 6050−6051.

(2) Tan, Z. K.; Moghaddam, R. S.; Lai, M. L.; Docampo, P.; Higler, R.; Deschler, F.; Price, M.; Sadhanala, A.; Pazos, L. M.; Credgington, D.; Hanusch, F.; Bein, T.; Snaith, H. J.; Friend, R. H. Bright Light-Emitting Diodes Based on Organometal Halide Perovskite. *Nat. Nanotechnol.* **2014**, *9*, 687−692.

(3) Wei, Q.; Li, X.; Liang, C.; Zhang, Z.; Guo, J.; Hong, G.; Xing, G.; Huang, W. Recent Progress in Metal Halide Perovskite Micro- and Nanolasers. *Adv. Opt. Mater.* **2019**, *7*, 1900080.

(4) Xing, G.; Mathews, N.; Lim, S. S.; Yantara, N.; Liu, X.; Sabba, D.; Grätzel, M.; Mhaisalkar, S.; Sum, T. C. Low-Temperature Solution-Processed Wavelength-Tunable Perovskites for Lasing. *Nat. Mater.* **2014**, *13*, 476−480.

(5) Cho, H.; Jeong, S. H.; Park, M. H.; Kim, Y. H.; Wolf, C.; Lee, C. L.; Heo, J. H.; Sadhanala, A.; Myoung, N. S.; Yoo, S.; Im, S. H.; Friend, R. H.; Lee, T. W. Overcoming the Electroluminescence Efficiency Limitations of Perovskite Light-Emitting Diodes. *Science* **2015**, *350*, 1222−1225.
(6) Veldhuis, S. A.; Boix, P. P.; Yantara, N.; Li, M.; Sum, T. C.; Mathews, N.; Mhaisalkar, S. G. Perovskite Materials for Light-Emitting Diodes and Lasers. *Adv. Mater.* **2016**, *28*, 6804−6834.
(7) Li, Z.; Chen, Z.; Yang, Y.; Xue, Q.; Yip, H. L.; Cao, Y. Modulation of Recombination Zone Position for Quasi-Two-Dimensional Blue Perovskite Light-Emitting Diodes with Efficiency Exceeding 5%. *Nat. Commun.* **2019**, *10*, 1027.
(8) Lin, K.; Xing, J.; Quan, L. N.; de Arquer, F. P. G.; Gong, X.; Lu, J.; Xie, L.; Zhao, W.; Zhang, D.; Yan, C.; Li, W.; Liu, X.; Lu, Y.; Kirman, J.; Sargent, E. H.; Xiong, Q.; Wei, Z. Perovskite Light-Emitting Diodes with External Quantum Efficiency Exceeding 20 per Cent. *Nature* **2018**, *562*, 245−248.
(9) Cao, Y.; Wang, N.; Tian, H.; Guo, J.; Wei, Y.; Chen, H.; Miao, Y.; Zou, W.; Pan, K.; He, Y.; Cao, H.; Ke, Y.; Xu, M.; Wang, Y.; Yang, M.; Du, K.; Fu, Z.; Kong, D.; Dai, D.; Jin, Y.; Li, G.; Li, H.; Peng, Q.; Wang, J.; Huang, W. Perovskite Light-Emitting Diodes Based on Spontaneously Formed Submicrometre-Scale Structures. *Nature* **2018**, *562*, 249−253.
(10) Zhao, X.; Tan, Z. K. Large-Area near-Infrared Perovskite Light-Emitting Diodes. *Nat. Photonics* **2020**, *14*, 215.
(11) Wang, Q.; Wang, X.; Yang, Z.; Zhou, N.; Deng, Y.; Zhao, J.; Xiao, X.; Rudd, P.; Moran, A.; Yan, Y.; Huang, J. Efficient Sky-Blue Perovskite Light-Emitting Diodes via Photoluminescence Enhancement. *Nat. Commun.* **2019**, *10*, 5639.
(12) Stranks, S. D.; Eperon, G. E.; Grancini, G.; Menelaou, C.; Alcocer, M. J. P.; Leijtens, T.; Herz, L. M.; Petrozza, A.; Snaith, H. J. Electron-Hole Diffusion Lengths Exceeding. *Science* **2013**, *342*, 341−345.
(13) Xing, G.; Mathews, N.; Lim, S. S.; Lam, Y. M.; Mhaisalkar, S.; Sum, T. C. Long-Range Balanced Electron- and Hole-Transport Lengths in Organic-Inorganic $CH_3NH_3PbI_3$. *Science* **2013**, *342*, 344−347.
(14) Xing, G.; Wu, B.; Wu, X.; Li, M.; Du, B.; Wei, Q.; Guo, J.; Yeow, E. K. L.; Sum, T. C.; Huang, W. Transcending the Slow Bimolecular Recombination in Lead-Halide Perovskites for Electroluminescence. *Nat. Commun.* **2017**, *8*, 14558.
(15) Song, J.; Fang, T.; Li, J.; Xu, L.; Zhang, F.; Han, B.; Shan, Q.; Zeng, H. Organic−Inorganic Hybrid Passivation Enables Perovskite QLEDs with an EQE of 16.48%. *Adv. Mater.* **2018**, *30*, 1805409.
(16) Yan, F.; Xing, J.; Xing, G.; Quan, L.; Tan, S. T.; Zhao, J.; Su, R.; Zhang, L.; Chen, S.; Zhao, Y.; Huan, A.; Sargent, E. H.; Xiong, Q.; Demir, H. V. Highly Efficient Visible Colloidal Lead-Halide Perovskite Nanocrystal Light-Emitting Diodes. *Nano Lett.* **2018**, *18*, 3157−3164.
(17) Han, D.; Imran, M.; Zhang, M.; Chang, S.; Wu, X. G.; Zhang, X.; Tang, J.; Wang, M.; Ali, S.; Li, X.; Yu, G.; Han, J.; Wang, L.; Zou, B.; Zhong, H. Efficient Light-Emitting Diodes Based on in Situ Fabricated $FAPbBr_3$ Nanocrystals: The Enhancing Role of the Ligand-Assisted Reprecipitation Process. *ACS Nano* **2018**, *12*, 8808−8816.
(18) Wang, N.; Cheng, L.; Ge, R.; Zhang, S.; Miao, Y.; Zou, W.; Yi, C.; Sun, Y.; Cao, Y.; Yang, R.; Wei, Y.; Guo, Q.; Ke, Y.; Yu, M.; Jin, Y.; Liu, Y.; Ding, Q.; Di, D.; Yang, L.; Xing, G.; Tian, H.; Jin, C.; Gao, F.; Friend, R. H.; Wang, J.; Huang, W. Perovskite Light-Emitting Diodes Based on Solution-Processed Self-Organized Multiple Quantum Wells. *Nat. Photonics* **2016**, *10*, 699−704.
(19) Liang, C.; Zhao, D.; Li, Y.; Li, X.; Peng, S.; Shao, G.; Xing, G. Ruddlesden-Popper Perovskite for Stable Solar Cells. *Energy Environ. Mater.* **2018**, *1*, 221−231.
(20) Pang, S.; Hu, H.; Zhang, J.; Lv, S.; Yu, Y.; Wei, F.; Qin, T.; Xu, H.; Liu, Z.; Cui, G. $NH_2CH = NH_2PbI_3$: An Alternative Organolead Iodide Perovskite Sensitizer for Mesoscopic Solar Cells. *Chem. Mater.* **2014**, *26*, 1485−1491.
(21) Yang, X.; Zhang, X.; Deng, J.; Chu, Z.; Jiang, Q.; Meng, J.; Wang, P.; Zhang, L.; Yin, Z.; You, J. Efficient Green Light-Emitting Diodes Based on Quasi-Two-Dimensional Composition and Phase Engineered Perovskite with Surface Passivation. *Nat. Commun.* **2018**, *9*, 1169.
(22) Tu, Y. G.; Xu, G. N.; Yang, X. Y.; Zhang, Y. F.; Li, Z. J.; Su, R.; Luo, D. Y.; Yang, W. Q.; Miao, Y.; Cai, R.; Jiang, L. H.; Du, X. W.; Yang, Y. C.; Liu, Q. S.; Gao, Y.; Zhao, S.; Huang, W.; Gong, Q. H.; Zhu, R. Mixed-Cation Perovskite Solar Cells in Space. *Sci. China: Phys., Mech. Astron.* **2019**, *62*, 1169.
(23) Zhang, X.; Liu, H.; Wang, W.; Zhang, J.; Xu, B.; Karen, K. L.; Zheng, Y.; Liu, S.; Chen, S.; Wang, K.; Sun, X. W. Hybrid Perovskite Light-Emitting Diodes Based on Perovskite Nanocrystals with Organic-Inorganic Mixed Cations. *Adv. Mater.* **2017**, *29*, 1606405.
(24) Liu, T.; Zong, Y.; Zhou, Y.; Yang, M.; Li, Z.; Game, O. S.; Zhu, K.; Zhu, R.; Gong, Q.; Padture, N. P. High-Performance Formamidinium-Based Perovskite Solar Cells via Microstructure-Mediated δ-to-α Phase Transformation. *Chem. Mater.* **2017**, *29*, 3246−3250.
(25) Li, Z.; Yang, M.; Park, J. S.; Wei, S. H.; Berry, J. J.; Zhu, K. Stabilizing Perovskite Structures by Tuning Tolerance Factor: Formation of Formamidinium and Cesium Lead Iodide Solid-State Alloys. *Chem. Mater.* **2016**, *28*, 284−292.
(26) Wang, Z.; Lin, Q.; Chmiel, F. P.; Sakai, N.; Herz, L. M.; Snaith, H. J. Efficient Ambient-Air-Stable Solar Cells with 2D-3D Heterostructured Butylammonium-Caesium-Formamidinium Lead Halide Perovskites. *Nat. Energy* **2017**, *2*, 17135.
(27) Xiao, M.; Huang, F.; Huang, W.; Dkhissi, Y.; Zhu, Y.; Etheridge, J.; Gray-Weale, A.; Bach, U.; Cheng, Y. B.; Spiccia, L. A Fast Deposition-Crystallization Procedure for Highly Efficient Lead Iodide Perovskite Thin-Film Solar Cells. *Angew. Chem., Int. Ed.* **2014**, *53*, 9898−9903.
(28) Shang, Y.; Li, G.; Liu, W.; Ning, Z. Quasi-2D Inorganic $CsPbBr_3$ Perovskite for Efficient and Stable Light-Emitting Diodes. *Adv. Funct. Mater.* **2018**, *28*, 1801193.
(29) Xing, J.; Zhao, Y.; Askerka, M.; Quan, L. N.; Gong, X.; Zhao, W.; Zhao, J.; Tan, H.; Long, G.; Gao, L.; Yang, Z.; Voznyy, O.; Tang, J.; Lu, Z. H.; Xiong, Q.; Sargent, E. H. Color-Stable Highly Luminescent Sky-Blue Perovskite Light-Emitting Diodes. *Nat. Commun.* **2018**, *9*, 3541.
(30) Quan, L. N.; Zhao, Y.; García de Arquer, F. P.; Sabatini, R.; Walters, G.; Voznyy, O.; Comin, R.; Li, Y.; Fan, J. Z.; Tan, H.; Pan, J.; Yuan, M.; Bakr, O. M.; Lu, Z.; Kim, D. H.; Sargent, E. H. Tailoring the Energy Landscape in Quasi-2D Halide Perovskites Enables Efficient Green-Light Emission. *Nano Lett.* **2017**, *17*, 3701−3709.

https://dx.doi.org/10.1021/acs.jpclett.0c01252
J. Phys. Chem. Lett. 2020, 11, 5877−5882